Hydro-elasto-plastic modelling with a solid/fluid transition

Zhaohua Li, Frédéric Dufour, Félix Darve

Hydro-elasto-plastic modelling with a solid/fluid transition

Zhaohua Li, Frédéric Dufour *, Félix Darve

Grenoble-INP/Univ. Joseph Fourier/CNRS UMR 5521, 3SR Laboratory, Grenoble, France

This paper deals with a new model for solving coupled hydromechanical problems, based on an existing unified model. Firstly, the unified model for granular media, describing solid and fluid states with the transition between them, is briefly presented and extended to the unsaturated domain using Bishop's effective stress. Secondly, an adapted stress–strain relationship is derived from modified Van Genuchten–Mualem's water retention curves. On this basis, a finite element formulation with Lagrangian integration points in a visco-elasto-plastic framework is proposed and implemented in a FEMLIP tool. Finally, the formulation is validated with reference to several benchmarks. The results and analysis show its reliability, and by means of FEMLIP, more complex and realistic problems are expected to be solved in the field of natural risks.

1. Introduction

In the early history of soil mechanics, researchers generally focused on the study of dry or saturated soils, so most soil mechanics theories can only apply to these conditions. As knowledge improved, increasing phenomena were observed related to the unsaturation of soils. Actually, as is well known, unsaturation gives soil several significant features such as enhanced strength, increasing fragility and plastic collapse along with wetting processes under certain stress levels. In the past few decades, there has been an increasing interest in the study of coupled hydromechanical problems in geomaterial porous media. Alonso et al. [4] were the first to provide a complete elasto-plastic framework for unsaturated soil; then a large number of constitutive models, giving more or less schematized stress–strain relationships, were established [5–7]. In recent years, more highly developed models have included suction–saturation relationships [34], such as the models proposed by Gallipoli et al. [8], Wheeler et al. [11], Tarrantino et al. [12], and Sheng et al. [35]. All these models have taken into account the water retention curves with a hydraulic hysteresis.

The above-mentioned constitutive models elaborate the solid-like behaviour of geomaterials. However, saturated loose geomaterials generally exhibit a fluid-like behaviour with a burst of kinetic energy in the postfailure stage. An example is the onset and propagation of a flow-type landslide. To describe such geomaterials comprehensively and completely, a unified model that consists of appropriate solid-like and fluid-like models and a criterion of solid–fluid transition is required. Recently, a unified model, in which solid-like behaviour and fluid-like behaviour are described by the PLASOL elasto-plastic model [9] and the Bingham viscous model, respectively, while Hill's second-order work criterion [13] is chosen as the criterion of transition, has been established [10,28]. In this paper, this model will be extended to unsaturated conditions.

A such simulation of complete solid–fluid behaviours requires solving large transformation problems. Several mesh-free methods are considered herein, such as smoothed particle hydrodynamics (SPH) [42] and the material point method (MPM) [43]. Because it has the advantage of tracking the history of the variables involved in elasto-plasticity and describing large transformations, the finite element method with Lagrangian integration points (FEMLIP), developed from "Particle-in-Cell" method [33], is used in this paper.

This paper proceeds as follows. In Section 2 the unified model is briefly introduced, and the adapted effective stress and modified Van Genuchten's water retention curves are specified. Section 3 establishes the derivation of stress–strain relations and the finite element formulation. The global visco-elasto-plastic constitutive relation in a hydromechanical framework presents all the informations for the computations in Ellipsis, the code based on the FEMLIP method. Section 4 gives three benchmarks to discuss and validates the readability of Ellipsis for solving hydromechanical problems. Finally, in Section 5, conclusions are drawn and future prospects are discussed.

Nomenclature

Exponents and index

$\overline{(.)}$	net value
$(.)', (.)_{eff}$	effective value
$(.)_0, (.)^0$	initial value
$(.)_f$	final value
$(.)^t$	current value
$\dot{(.)}$	temporal differential
$(.)^T$	transposition
$(.)_{tot}$	total value
$(.)_v$	viscous value
$(.)_e$	elastic value
$(.)_p$	plastic value
$(.)_n$	numerical value

Scalars

c	cohesion
ϕ_c	mobilised friction angle under triaxial compression paths
ϕ_e	mobilised friction angle under triaxial extension paths
$J_{1\sigma'}, J_{2\sigma}, J_{3\sigma}$	effective stress tensor invariants
d^2w	local second-order work
D^2W	global second-order work
ω_i	numerical weight of integration point i
J_i	determinant of Jacobian matrix
s_y	Bingham yield stress
η	dynamic viscosity
χ	parameter of Bishop's effective stress
$a_\chi,\ n_\chi$	parameters of χ
$u_a,\ u_w$	air pressure and water pressure
s	suction
s_{aev}	air entry value
P_{atm}	atmospheric pressure
Sr	degree of saturation
θ	water content
$a_v,\ n_v$	parameters of Van Genuchten–Mualem's WRCs
$k,\ \lambda$	constant material parameters
n	porosity
t	time
q	Darcy's velocity normal to boundary
S	boundary subjected to force
S_w	boundary subjected to water flux
V	volume considered
g	gravity acceleration
ρ	density
ρ_w	water density
K	bulk modulus
μ	elastic shear modulus
ν	Poisson's coefficient
p	total mean pressure
k_r	relative hydraulic conductivity

Vectors

$\boldsymbol{V_k}$	Darcy's velocity
$\boldsymbol{f}$	boundary force vector
$\boldsymbol{b}$	body force vector
$\boldsymbol{b_w}$	body force vector of pore water
$\boldsymbol{U}$	nodal displacement vector
$\boldsymbol{U_w}$	nodal water pressure vector
$\boldsymbol{N_w}$	water pressure shape function

Tensors

$\boldsymbol{D^{ep}}$	elasto-plastic matrix
$\boldsymbol{D^{v}}$	viscous matrix
$\boldsymbol{D^{ve}}$	visco-elastic matrix
$\boldsymbol{\sigma}$	total stress tensor
$\boldsymbol{\varepsilon}$	strain tensor
$\boldsymbol{\tau}$	deviatoric stress tensor
$\boldsymbol{e}$	deviatoric strain tensor
$\boldsymbol{k}$	unsaturated permeability tensor
$\boldsymbol{k_s}$	saturated permeability tensor
$\boldsymbol{N}$	velocity shape function

2. A unified solid–fluid model incorporating hydromechanical coupling

Fine soils are known to exhibit elasto-plastic behaviour as solids and viscous behaviour as fluids alternatively. To model an entire process of the geomaterial loss of stability, an existing unified model in 3D, describing the solid, fluid states with a transition between them is taken into account. For greater detail on this model, the reader can refer to Prime et al. [2,10,28]. To solve hydromechanical problems, this model is extended here for partially saturated conditions by introducing Bishop's effective stress and a water-retention model.

2.1. Elasto-plastic model with a hydromechanical coupling

2.1.1. Bishop's effective stress

The discussion on the choice of the proper stress variables in unsaturated conditions is still open. For greater detail, the reader can refer to [22,23]. In this paper, Bishop's effective stress, expressed as follows, is used in the elasto-plastic model to simulate the solid behaviour of unsaturated soils:

$$\boldsymbol{\sigma}' = \boldsymbol{\sigma} - u_a\boldsymbol{m} + \chi(u_a - u_w)\boldsymbol{m} \tag{1}$$

where $\boldsymbol{\sigma}'$ is the effective intergranular stress vector, $\boldsymbol{\sigma}$ the total stress vector, u_a the isotropic air pressure, and u_w the isotropic water pressure. $\boldsymbol{m^T} = (1,1,1,0,0,0)$ and $s = u_a - u_w$ is the suction component. A six-component vectorial rotation is used for σ and σ'.

Determining χ is a delicate point. Besides the most common formulation $\chi = Sr$ [24], many researchers have studied and proposed several expressions for this parameter, such as Khalili and Khabbaz [25] and Alonso et al. [26]. Arairo et al. [27] proposed the following expression on the basis of Alonso's work:

$$\chi = \left(1 + \left(\frac{a_\chi s}{P_{atm}}\right)^{n_\chi}\right)^{\frac{1}{n_\chi}-1} \tag{2}$$

where a_χ and n_χ are parameters defined to ensure that the value of χ is always located between two boundary water retention curves for a given suction value. By adjusting the two parameters, many features of unsaturated soils can be described including plastic collapse in the wetting process [27]. Let us note, however, that the most recent advances in unsaturated granular media have shown the tensorial nature of χ [38,39].

2.1.2. PLASOL constitutive relation

In the solid stage, the behaviour of unsaturated geomaterials is described by the PLASOL non-associated elasto-plastic model by means of Bishop's effective stress mentioned above. This model, appropriate to deal with a wide range of diversified soils, was developed at Liege University; more detailed information is

provided by Barnichon [9]. Let us introduce its main features synoptically.

Firstly, a Van Eekelen plastic criterion [14], which is close to the Mohr–Coulomb plastic criterion but avoids geometric singularities, is chosen as the plastic limit in this model. In the 3D principal stress framework, the expression of the Van Eekelen yield criterion is stated with the three effective stress tensor invariants $J_{1\sigma'} = \mathrm{tr}(\boldsymbol{\sigma}')$, $J_{2\sigma} = \sqrt{\mathrm{tr}(\boldsymbol{\tau}^2)}$ and $J_{3\sigma} = \sqrt[3]{\mathrm{tr}(\boldsymbol{\tau}^3)}$ $\left(\boldsymbol{\tau} = \boldsymbol{\sigma}' - \frac{1}{3}\mathrm{tr}(\boldsymbol{\sigma}')\right)$ as follows:

$$f = J_{2\sigma} + m\left(J_{1\sigma'} - \frac{3c}{\tan\varphi_c}\right) = 0 \tag{3}$$

where c is the cohesion, φ_c is the mobilised friction angle under triaxial compression paths, and m is a coefficient depending on the Lode angle and the friction angles.

Secondly, PLASOL proposes a way to model the hardening of the yield surface during loading. With the Von Mises equivalent plastic strain $E^p_{eq} = \sqrt{\frac{2}{3}e^p_{ij}e^p_{ij}}$, $\left(\boldsymbol{e}^p = \boldsymbol{\varepsilon}^p - \frac{\boldsymbol{I}}{3}\mathrm{tr}(\boldsymbol{\varepsilon}^p)\right)$, three internal variables (compression, extension friction angles and cohesion), expressed as follows, evolve between the elastic initial values $(c_0, \varphi_{e0}, \varphi_{c0})$ and the plastic limit values $(c_f, \varphi_{ef}, \varphi_{cf})$ during the plastic regime.

$$\begin{cases} \varphi_c = \varphi_{c0} + \frac{(\varphi_{cf}-\varphi_{c0})E^p_{eq}}{B_p + E^p_{eq}} \\ \varphi_e = \varphi_{e0} + \frac{(\varphi_{ef}-\varphi_{e0})E^p_{eq}}{B_p + E^p_{eq}} \\ c = c_0 + \frac{(c_f-c_0)E^p_{eq}}{B_c + E^p_{eq}} \end{cases} \tag{4}$$

where B_c and B_p are hardening parameters, corresponding to the values of the equivalent plastic strains for which half of the hardening on friction angles and cohesion is reached.

As illustrated in Fig. 3, the plastic criterion of the Van Eekelen type represents a conical surface, making it possible to describe two important features of cohesive–frictional geomaterials: the increase of strength with confinement and the higher strength for extension triaxial stress loading compared with the Mohr–Coulomb criterion. Finally, 13 parameters [15] are required to describe an elasto-plastic soil using the PLASOL constitutive law.

2.1.3. Water-retention behaviour

The water retention curve (WRC) that links suction to the degree of saturation or water content is an important aspect of unsaturated soil properties in the solid state. Generally, the degree of saturation on the drying curve is always greater than that on the wetting curve, for a given suction value. This phenomenon (soil exhibits different suction–degree of saturation relations during the drying and wetting processes) is considered as hydraulic hysteresis. Strictly speaking, the WRCs are made up of four types of curves as shown in Fig. 1: the boundary drying curve, boundary wetting curve, wetting scanning curves and drying scanning curves.

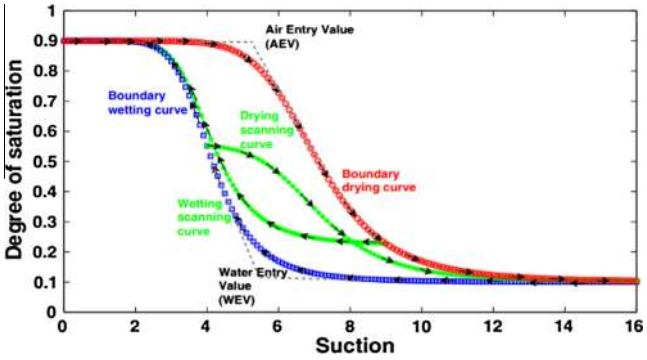

Fig. 1. Scheme of WRC with the four families of curves: the two boundary drying and wetting curves and the scanning curves.

In order to improve the capacity of the unified model to solve the hydromechanical problems, the WRCs proposed by Van Genuchten–Mualem are taken into account. According to Van Genuchten [3], and introducing the atmospheric pressure P_{atm}, the boundary WRCs are expressed as:

$$Sr_v = Sr_{res} + (Sr_{sat} - Sr_{res})\left(1 + \left(\frac{a_v s}{P_{atm}}\right)^{n_v}\right)^{\frac{1}{n_v}-1} \tag{5}$$

where the index v is w in case of a wetting process and becomes d for the drying process; Sr_{res}, Sr_{sat} and Sr_v mean, respectively, the residual, saturated and current degrees of saturation; a_v is a parameter involving the air entry value (AEV), n_v is principally related to the variation of water content in the soil once the suction value exceeds the AEV.

In the approach developed by Arairo et al. [27], the Van Genuchten's WRC is extended by considering the dependence of Van Genuchten parameters on porosity. The following expression is proposed:

$$s_{aev} = s_{aev0}\exp\left(\lambda\left(\frac{1}{n} - \frac{1}{n_0}\right)\right) \tag{6}$$

where s_{aev} is the AEV, s_{aev0} is a reference AEV for a reference porosity n_0 and λ a constant material parameter. Hence, once the AEV has been refreshed, a_v is then updated by the expression:

$$a_v = \frac{P_{atm}}{s_{aev}}\left(\frac{n_v-1}{n_v}\right)^{\frac{1}{n_v}}\frac{-n_v}{(n_v-1)^2}\left(\left(\frac{2n_v-1}{n_v}\right)^{2-\frac{1}{n_v}} - \left(\frac{2n_v-1}{n_v}\right) - \frac{(n_v-1)^2}{n_v}\right) \tag{7}$$

Besides, by introducing Mualem's scanning curves [27,44], the hysteresis can be considered in our model. A hydro-elasto-plastic model has thus been established for simulating the solid behaviour of unsaturated geomaterials.

2.2. Solid–fluid transition

In certain conditions, soils can lose their strength, and an infinitesimal additional load at an extremum stress leads to a large response, which means a loss of stability. This phenomenon is considered to link the solid and fluid states [20]. Besides the classic plasticity criterion, there are various modes of failure constituting a potential failure domain called the bifurcation domain [16]. There are two modes classically highlighted: localised and diffuse modes. The former, leading to a concentration of the plastic strains in a shear band as shown in Fig. 2(a), has been thoroughly studied. The latter does not present any localisation phenomenon but generally causes a global disorganisation in samples, as illustrated in Fig. 2(b). Fig. 2(c) shows a classical stress path in an undrained triaxial test of a loose sand. Along with this stress path, a diffuse failure occurs at q peak strictly inside the Mohr–Coulomb plastic limit, if the undrained path is axially force controlled.

The diffuse failure can explain many instability cases, for instance the most significant, the liquefaction of loose sand. According to recent studies, diffuse failure can occur without reaching the plastic limit criterion or the localisation criterion. This conclusion has been proven theoretically, experimentally, and numerically [16–20].

Consequently, instead of using a plasticity criterion or a localisation criterion, the loss of stability is checked once the effective stress state is inspected to overstep the lower limit of the bifurcation domain. The instability leading to localised or diffuse failure is judged by the Hill's criterion [13], written as:

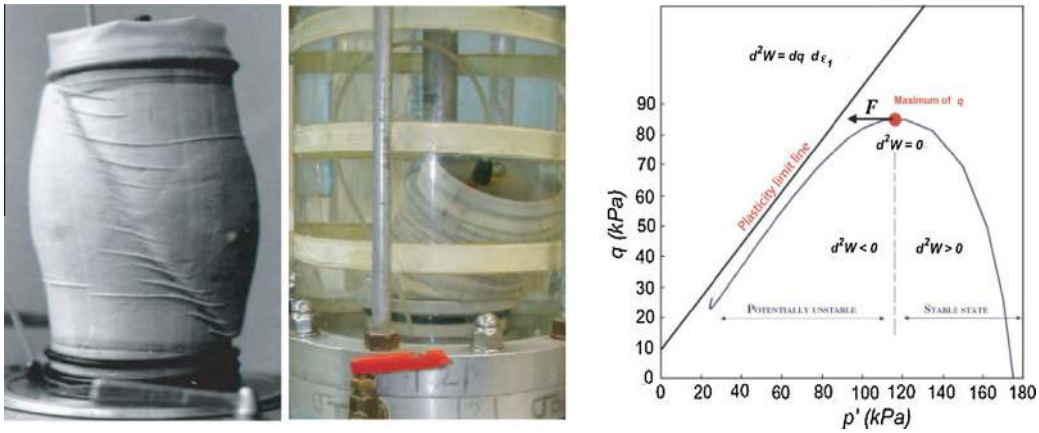

Fig. 2. (a) Localised failure in drained triaxial test, (b) diffuse failure in undrained triaxial test, (c) stress path in an undrained triaxial test of a loose sand.

$$d^2w = d\sigma'_{ij}d\varepsilon_{ij} \tag{8}$$

The second-order work is checked locally at all integration points of the domain studied. To improve the readability of the d^2w graphs, d^2w is treated by normalisation:

$$d^2w_i^{norm} = \frac{d^2w_i}{\|d\boldsymbol{\sigma}'_i\|\|d\boldsymbol{\varepsilon}_i\|} \tag{9}$$

where $\|d\boldsymbol{\sigma}'_i\|$ and $\|d\boldsymbol{\varepsilon}_i\|$ are, respectively, the norms of the stress increment and the strain increment of the integration point *i*. In this way, the d^2w value is limited between -1 and 1. If $d^2w > 0$, the particle is considered as stable; otherwise, a local diffuse or localised failure may be reached.

Furthermore, Hill [13] proposed a global second-order work criterion for a boundary value problem. With a global $D^2W > 0$, written as follows, the body can be considered globally stable [37], if:

$$D^2W = \frac{\sum\left(d^2w_i\omega_iJ_i\right)}{\sum\omega_iJ_i\sum\|d\boldsymbol{\sigma}'_i\|\|d\boldsymbol{\varepsilon}_i\|} > 0 \tag{10}$$

where ω_i is the numerical weight of integration point i,J_i corresponds to the determinant of the Jacobian matrix, and D^2W is the normalised global second order work.

2.3. Bingham's viscous law

For geomaterial particles, once $d^2w \leqslant 0$, for at least one loading direction, the particle is seated in the bifurcation domain. If $d^2w \leqslant 0$ for the current incremental stresses and strains, the particle is considered to be in a transition state between solid and fluid. For the present unified model, the non-linearity of the viscous relation and the dependency of the stress threshold to the confinement are neglected for the sake of simplicity. Hence, the simulated geomaterials exhibit a viscous behaviour obeying Bingham's law. In three dimensions, considering the expression of Duvaut and Lions [36] and Balmforth and Craster [21], Bingham's viscous law can be written as follows:

$$\text{if } J_{2\sigma} > s_y: \quad \dot{e}_{ij} = \frac{1}{2\eta}\left(\tau_{ij} - s_y\frac{\tau_{ij}}{J_{2\sigma}}\right) = \frac{J_{2\sigma} - s_y}{2\eta}\cdot\frac{\tau_{ij}}{J_{2\sigma}}, \quad \text{else}: \quad \dot{e}_{ij} = 0 \tag{11}$$

where $J_{2\sigma}$ is the second invariant of the stress tensor, s_y is the Bingham yield stress, η is the dynamic viscosity and τ and $\dot{e}$ are, respectively, the deviatoric stress and strain rate tensors. It should be noted that, in our hydromechanical model, it's the stress deviator that is used to compare with s_y.

In conclusion, the saturated or unsaturated porous medium considered obeys an elasto-plastic model described by the PLASOL law, the hydromechanical coupling is considered by means of Bishop's effective stress and the modified Van Genuchten–Mualem model. For appropriate stress levels, it is checked by Hill's second-order work criterion and the yield stress of Bingham's viscous law. Once failure occurs, the medium behaves as a fluid and large displacements appear. The check by the second-order work is irreversible but this is not the case for the yield stress. If $J_{2\sigma} < s_y$ in the fluid state, the medium returns to the solid state, obeying the elasto-plastic behaviour. The unified model in 3D in the principal stress frame is illustrated in Fig. 3, and in Fig. 4, a common framework is illustrated in 1D. This framework consists of three components: an elasto-plastic model, a viscous model and a failure criterion of the second-order work in between.

3. Finite element implementation

3.1. Incremental constitutive relations

With given materials, an appropriate incremental stress–strain relation needs to be developed in order to integrate it using a numerical method to solve boundary value problems. For unsaturated soils, the incremental relation is summarised in [40]:

$$\begin{pmatrix} d\boldsymbol{\sigma}' \\ ds \end{pmatrix} = \begin{pmatrix} \boldsymbol{D}^{ep} & \boldsymbol{W}^{ep} \\ \boldsymbol{R} & G \end{pmatrix}\begin{pmatrix} d\boldsymbol{\varepsilon} \\ dSr \end{pmatrix} \tag{12}$$

Let us note here that, according to multi-phase material mechanics, the net stress tensor $\overline{\boldsymbol{\sigma}} = \boldsymbol{\sigma} - u_a\boldsymbol{m}$ cannot be considered as a proper constitutive variable, while the effective stress and the suction are related to the granular skeleton and the isotropic fluid pressures (water and air), respectively.

As FEMLIP was initially developed based on the viscous frame, in which the stress–strain relationship is stated as $\boldsymbol{\sigma} = \boldsymbol{D}^v\dot{\boldsymbol{\varepsilon}}$, Moresi extended it into the visco-elasticity framework [30], by introducing two parameters that contain viscous and elastic moduli:

$$\eta_{eff} = \frac{1}{\frac{1}{\eta} + \frac{1}{\mu\Delta t_e}}, \quad K_{eff} = \frac{1}{\frac{1}{K_v} + \frac{1}{K_e\Delta t_e}} \tag{13}$$

The visco-elastic relationship in FEMLIP is therefore stated as: $\Delta\boldsymbol{\sigma} = D^{ve}\dot{\boldsymbol{\varepsilon}}$, with a temporal discretisation by Δt_e. This relation can be expressed as:

$$\boldsymbol{\sigma}'^{t+\Delta t_e} = \boldsymbol{D}^{ve}\dot{\boldsymbol{\varepsilon}}^{t+\Delta t_e} + \boldsymbol{\sigma}'^{t} \tag{14}$$

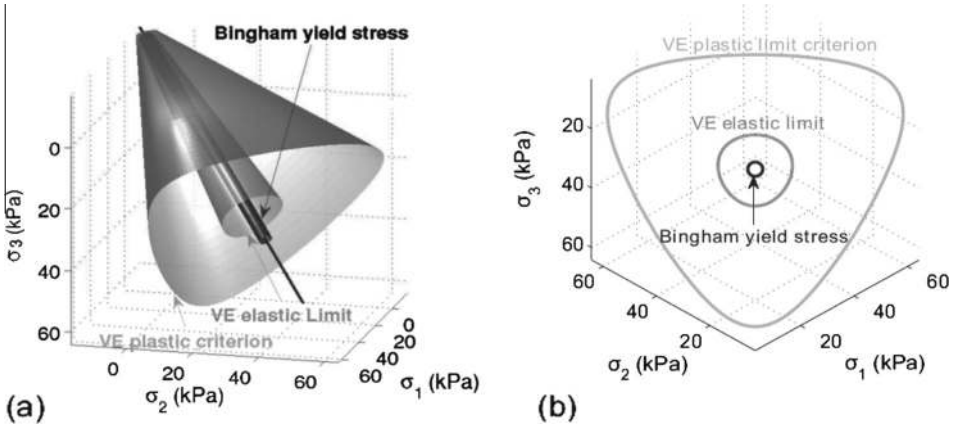

Fig. 3. Unified model in the principal stress frame ("VE" means Van Eekelen) (a) 3D view and (b) deviatoric stress plane view.

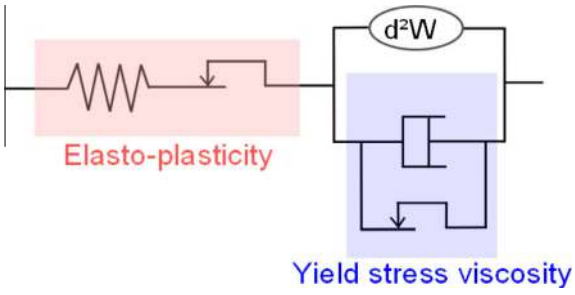

Fig. 4. Common scheme of the unified model in one dimension.

where $\boldsymbol{D}^{ve}$ is the visco-elastic matrix. In this paper, in consideration of hydromechanical coupling, Bishop's effective stress relation (1) is used. Expression (14) becomes:

$$\overline{\boldsymbol{\sigma}}^{t+\Delta t_e} = \boldsymbol{D}^{ve}\dot{\boldsymbol{\varepsilon}}^{t+\Delta t_e} - (\chi s)^{t+\Delta t_e}\boldsymbol{m} + \boldsymbol{\sigma}'^{t} \tag{15}$$

For a unified form with a water content-suction relation, this relation can be expressed with a transformation $s^{t+\Delta t_e} = \Delta t_e \dot{s}^{t+\Delta t_e} + s^t$, as follows:

$$\overline{\boldsymbol{\sigma}}^{t+\Delta t_e} = \boldsymbol{D}^{ve}\dot{\boldsymbol{\varepsilon}}^{t+\Delta t_e} - \Delta t_e \chi \dot{s}^{t+\Delta t_e}\boldsymbol{m} - \chi s^t \boldsymbol{m} + \boldsymbol{\sigma}'^{t} \tag{16}$$

It should be noted that, for the sake of simplification, χ is assumed to be constant for a sufficiently small Δt_e, and is effectively updated in computation at each time step. Consequently, a general stress–strain relationship in the hydromechanical visco-elastic framework is established.

With the Van Genuchten–Mualem WRCs introduced in Eq. (5), the suction–water content relation is given by (knowing that $\theta = n \cdot Sr$):

$$\begin{aligned} d\theta &= Srdn + ndSr = \left(Sr + n\frac{\partial Sr}{\partial n}\right)dn + n\frac{\partial Sr}{\partial s}ds \\ &= -(1-n)\left(Sr + n\frac{\partial Sr}{\partial n}\right)\boldsymbol{m}^T d\boldsymbol{\varepsilon} + n\frac{\partial Sr}{\partial s}ds \end{aligned} \tag{17}$$

Finally, the incremental stress–strain relationship implemented in the Ellipsis code can be expressed as:

$$\begin{pmatrix} \overline{\boldsymbol{\sigma}}^{t+\Delta t_e} \\ \dot{\theta}^{t+\Delta t_e} \end{pmatrix} = \begin{pmatrix} \boldsymbol{D}^{ve} & \boldsymbol{W} \\ \boldsymbol{T} & H \end{pmatrix} \begin{pmatrix} \dot{\boldsymbol{\varepsilon}}^{t+\Delta t_e} \\ \dot{s}^{t+\Delta t_e} \end{pmatrix} + \begin{pmatrix} -\chi s^t \boldsymbol{m} + \boldsymbol{\sigma}'^{t} \\ 0 \end{pmatrix} \tag{18}$$

where

$$\boldsymbol{W} = -\chi \boldsymbol{m} \Delta t_e$$

$$\boldsymbol{T} = -(1-n)\left(Sr + n\tfrac{\partial Sr}{\partial n}\right)\boldsymbol{m}^T$$

$$H = n\tfrac{\partial Sr}{\partial s}$$

In this relation, $\boldsymbol{D}^{ve}$ is a 6×6 matrix, $\boldsymbol{W}$ and $\boldsymbol{T}$ are a 6-element column vector and a 6-element row vector, respectively, and H is a scalar. It is obvious that H and $\boldsymbol{T}$ are classically derived from the modified Van Genuchten–Mualem's WRCs. According to Eqs. (5)–(7), $\frac{\partial Sr}{\partial s}$ and $\frac{\partial Sr}{\partial n}$ can be derived:

$$\frac{\partial Sr}{\partial s} = (Sr_{sat} - Sr_{res})(1-n_v)\frac{a_v}{P_{atm}}\left(1 + \left(\frac{a_v s}{P_{atm}}\right)^{n_v}\right)^{\frac{1}{n_v}-2}\left(\frac{a_v s}{P_{atm}}\right)^{n_v-1} \tag{19}$$

$$\begin{aligned} \frac{\partial Sr}{\partial n} = \frac{\partial Sr}{\partial a_v}\cdot\frac{\partial a_v}{\partial s_{aev}}\cdot\frac{\partial s_{aev}}{\partial n} &= \lambda(Sr_{sat} - Sr_{res})\left(1 + \left(\frac{a_v s}{P_{atm}}\right)^{n_v}\right)^{\frac{1}{n_v}-2}\left(\frac{a_v s}{P_{atm}}\right)^{n_v-1} \\ &\times \frac{s}{s_{aev}^2}\left(\frac{n_v-1}{n_v}\right)^{\frac{1}{n_v}-1}\frac{s_{aev0}}{n_0}\left(\frac{2n_v-1}{n_v}\right)^{2-\frac{1}{n_v}} - n_v\Bigg) \end{aligned} \tag{20}$$

The strain rate and the suction rate are both on the right side, so the velocity field and the pore water pressure can be solved firstly in the four corner nodes and in the central nodes, and the strain, stress and saturation field in material points can be determined later.

3.2. Global governing equations

As a three-phase mixed medium, the deformable unsaturated porous body consists of three phases (solid, liquid and gas) and four constituents (solid, water, vapour and dry air). To solve a multi-phase material problem, it is necessary to define the mechanical variables for each phase, to express the constitutive relation of each phase, the interaction laws between the phases, the equilibrium equations, the conservation laws and if necessary the balance of energy. In this paper, several hypothesis are taken into account to simplify the system of equations:

(1) The densities of liquid and solid grains are assumed to be constant. This means that the liquid and solid material phases are incompressible (but not the solid skeleton).
(2) The liquid flows in the connected voids of the medium following the generalised Darcy's law.
(3) Under atmospheric air pressure, the gas diffusion can be ignored, the air and water vapour pressures are considered nil (the pores are connected to the outside air).

(4) Under isothermal conditions, the heat transfer can be ignored, and the temperature field assumed to be constant.

Consequently, the governing equations consist of the equilibrium equation of momentum for the whole body, whose weak form can be written as:

$$\int_V (\partial \boldsymbol{\varepsilon}^T \boldsymbol{\sigma}) dV - \int_S (\partial \boldsymbol{u}^T \boldsymbol{f}) dS - \int_V (\partial \boldsymbol{u}^T \boldsymbol{b}) dV = 0 \tag{21}$$

and the continuity equation of water flow, which contains the conservation equation of water mass and the generalised Darcy's law, can be written as:

$$\mathrm{div}\left(-\frac{\boldsymbol{k}}{g}(\nabla \boldsymbol{u_w} - \boldsymbol{b_w})\right) + \frac{\partial}{\partial t}(\rho_w \theta) = 0 \tag{22}$$

where S and V are the boundary subjected to the distributed force $\boldsymbol{f}$ and the considered volume, respectively. $\boldsymbol{\sigma}$ is the Cauchy total stress tensor and $\boldsymbol{b}$ the body force vector. g is the gravity acceleration, ρ_w is the water density, $\boldsymbol{b}_w$ is the body force vector of pore water, $\boldsymbol{u}_w$ is the vector of pore water pressure, and $\boldsymbol{k}$ the unsaturated permeability tensor, written as $\boldsymbol{k} = k_r \cdot \boldsymbol{k_s}$. $\boldsymbol{k_s}$ is the anisotropic saturated permeability, and k_r the relative hydraulic conductivity. In our approach, the proposition by Van Genuchten [3] is used:

$$k_r = \frac{\left(1 - (\alpha_v s)^{n_v - 1}\left(1 + (\alpha_v s)^{n_v}\right)^{\frac{1}{n_v}-1}\right)^2}{\left(1 + (\alpha_v s)^{n_v}\right)^{\frac{1-\frac{1}{n_v}}{2}}} \tag{23}$$

This expression is derived from the Van Genuchten WRCs, so k_r is obviously influenced by the hydraulic hysteresis of unsaturated soils.

With appropriate shape functions, the velocity and pore water pressure fields can be approximated as:

$$\begin{cases} \dot{\boldsymbol{u}} = \boldsymbol{N}\dot{\boldsymbol{U}} \\ \dot{u}_w = \boldsymbol{N}_w \dot{\boldsymbol{U}}_w \end{cases} \tag{24}$$

where $\boldsymbol{N}$ and $\boldsymbol{N_w}$ are the shape function of velocity and pore water pressure, respectively.

According to the stress–strain and the water content–suction relations (18) in Section 3.1 and Eqs. (21), (22), (24):

$$\begin{cases} \int_V \boldsymbol{B}^T \boldsymbol{D}^{ve} \boldsymbol{B}\dot{\boldsymbol{U}}^{t+\Delta t_e} dV - \int_V \boldsymbol{B}^T \boldsymbol{W}\boldsymbol{N}_w \dot{\boldsymbol{U}}_w^{t+\Delta t_e} dV + \int_V \boldsymbol{B}^T \chi \boldsymbol{m} \boldsymbol{N}_w \boldsymbol{U}_w^t dV \\ \quad + \int_V \boldsymbol{B}^T \boldsymbol{\sigma}'^t dV = \int_S \boldsymbol{N}^T \boldsymbol{f}^{t+\Delta t_e} dS + \int_V \boldsymbol{N}^T \boldsymbol{b}^{t+\Delta t_e} dV \\ \int_V \boldsymbol{B}_w^T \frac{\boldsymbol{k}}{g\rho_w} \boldsymbol{B}_w \boldsymbol{U}_w^{t+\Delta t_e} dV + \int_V \boldsymbol{N}_w^T \boldsymbol{T}\boldsymbol{B}\dot{\boldsymbol{U}}^{t+\Delta t_e} dV - \int_V \boldsymbol{N}_w^T H \boldsymbol{N}_w \dot{\boldsymbol{U}}_w^{t+\Delta t_e} dV \\ \quad + \int_{S_w} \boldsymbol{N}_w^T q^{t+\Delta t_e} dS_w + \int_V \boldsymbol{B}_w^T \frac{\boldsymbol{k}}{g\rho_w} \boldsymbol{b}_w^{t+\Delta t_e} dV = 0 \end{cases} \tag{25}$$

where S_w is the boundary subjected to the water flux, $\boldsymbol{n}^T$ is a unit vector normal to surface S_w, $q = \boldsymbol{n}^T \boldsymbol{V}_k$ and $\boldsymbol{V}_k = -\frac{\boldsymbol{k}}{\rho_w g}(\nabla \boldsymbol{u}_w - \boldsymbol{b}_w)$ is the infiltration velocity. Finally, the discretised finite element equations are thus written in rate form:

$$\begin{pmatrix} \boldsymbol{A} & \boldsymbol{L} \\ \boldsymbol{L}' & \boldsymbol{S} \end{pmatrix} \begin{pmatrix} \dot{\boldsymbol{U}}^{t+\Delta t_e} \\ \dot{\boldsymbol{U}}_w^{t+\Delta t_e} \end{pmatrix} + \begin{pmatrix} 0 \\ \boldsymbol{R}\boldsymbol{U}_w^{t+\Delta t_e} \end{pmatrix} = \begin{pmatrix} \boldsymbol{F}^{t+\Delta t_e} - \boldsymbol{M}U_w^t \\ \boldsymbol{Q}_{ext}^{t+\Delta t_e} \end{pmatrix} \tag{26}$$

where

$$\begin{aligned} \boldsymbol{A} &= \textstyle\sum \int_V (\boldsymbol{B}^T \boldsymbol{D} \boldsymbol{B}) dV \\ \boldsymbol{L} &= -\textstyle\sum \int_V (\boldsymbol{B}^T \boldsymbol{W} \boldsymbol{N}_w) dV \\ \boldsymbol{M} &= \textstyle\sum \int_V (\boldsymbol{B}^T \chi \boldsymbol{m} \boldsymbol{N}_w) dV \\ \boldsymbol{F}^{t+\Delta t_e} &= \textstyle\sum \left(\int_V \left(\boldsymbol{N}^T \boldsymbol{b}^{t+\Delta t_e} - \boldsymbol{B}^T \boldsymbol{\sigma}'^t \right) dV + \int_S \left(\boldsymbol{N}^T \boldsymbol{t}^{t+\Delta t_e} \right) dS \right) \\ \boldsymbol{L}' &= \textstyle\sum \int_V \left(\boldsymbol{N}_w^T \boldsymbol{T} \boldsymbol{B} \right) dV \end{aligned}$$

$$\begin{aligned} \boldsymbol{S} &= -\textstyle\sum \int_V \left(\boldsymbol{N}_w^T H \boldsymbol{N}_w \right) dV \\ \boldsymbol{R} &= \textstyle\sum \int_V \left(\boldsymbol{B}_w^T \frac{\boldsymbol{k}}{g\rho_w} \boldsymbol{B}_w \right) dV \\ \boldsymbol{Q}_{ext}^{t+\Delta t_e} &= -\textstyle\sum \int_{S_w} \left(\boldsymbol{N}_w^T q^{t+\Delta t_e} \right) dS_w - \sum \int_V \left(\boldsymbol{B}_w^T \frac{\boldsymbol{k}}{g\rho_w} \boldsymbol{b}_w^{t+\Delta t_e} \right) dV \end{aligned}$$

The above equations make it possible to compute the velocity field and the pore water pressure rate.

By introducing $\dot{U}_w^{t+\Delta t_e} = \frac{U_w^{t+\Delta t_e} - U_w^t}{\Delta t_e}$, a convenient system of equations for solving the velocity and the pore water pressure fields in Ellipsis is obtained:

$$\begin{cases} \boldsymbol{A}\dot{\boldsymbol{U}}^{t+\Delta t_e} + \frac{\boldsymbol{L}}{\Delta t_e} \boldsymbol{U}_w^{t+\Delta t_e} = \boldsymbol{F}^{t+\Delta t_e} \\ \boldsymbol{L}'\dot{\boldsymbol{U}}^{t+\Delta t_e} + \left(\frac{\boldsymbol{S}}{\Delta t_e} + \boldsymbol{R} \right) \boldsymbol{U}_w^{t+\Delta t_e} = \boldsymbol{Q}_{ext}^{t+\Delta t_e} + \frac{\boldsymbol{S}}{\Delta t_e} \boldsymbol{U}_w^t \end{cases} \tag{27}$$

Now, a new formulation after the implantation of hydromechanical coupling is developed. With transformations, equation system (27) can be written as follows:

$$\hat{\boldsymbol{A}} \boldsymbol{U}_w^{t+\Delta t_e} = \hat{\boldsymbol{F}} \tag{28}$$

where

$$\begin{aligned} \hat{\boldsymbol{A}} &= \boldsymbol{L}' \boldsymbol{A}^{-1} \tfrac{\boldsymbol{L}}{\Delta t_e} - \left(\tfrac{\boldsymbol{S}}{\Delta t_e} + \boldsymbol{R} \right) \\ \hat{\boldsymbol{F}} &= \boldsymbol{L}' \boldsymbol{A}^{-1} \boldsymbol{F}^{t+\Delta t_e} - \left(\boldsymbol{Q}_{ext}^{t+\Delta t_e} + \tfrac{\boldsymbol{S}}{\Delta t_e} \boldsymbol{U}_w^t \right) \end{aligned}$$

To solve linearised Eq. (28) with a nonsymmetric matrix $\hat{\boldsymbol{A}}$, a new solver based on the biconjugate gradient stabilised method (BICGSTAB), instead of the conjugate gradient method, was implemented in the code. Developed by Van der Vorst [41], this method is based on the biconjugate gradient method (BiCG) but can inverse the nonsymmetric matrix and has faster and smoother convergence than the original BiCG and other variants.

3.3. Visco-elasto-plastic formulation in hydromechanical framework

Since Ellipsis was initially developed for geophysical problems involving viscous behaviour, elasticity and plasticity were implemented later. The global formulation was established by Dufour [1,30,31] and Prime et al. [2,10,28] as follows:

$$\begin{cases} \dot{\boldsymbol{e}}_{tot} - \dot{\boldsymbol{e}}_p = \dot{\boldsymbol{e}}_e + \dot{\boldsymbol{e}}_v = \frac{\dot{\boldsymbol{\tau}}}{2\mu'} + \frac{\boldsymbol{\tau}}{2\eta_n} + \frac{J_{2\sigma} - S_y}{J_{2\sigma}} \frac{\boldsymbol{\tau}}{2\eta} \\ \mathrm{tr}(\dot{\boldsymbol{\varepsilon}}_{tot}) - \mathrm{tr}(\dot{\boldsymbol{\varepsilon}}_p) = \mathrm{tr}(\dot{\boldsymbol{\varepsilon}}_e) + \mathrm{tr}(\dot{\boldsymbol{\varepsilon}}_v) = \frac{\dot{p}'}{K_e'} + \frac{p'}{K_v} \end{cases} \tag{29}$$

where $\dot{\boldsymbol{e}}$ is the deviatoric strain rate tensor, $\mathrm{tr}(\dot{\boldsymbol{\varepsilon}})$ is the volumic strain rate, $\boldsymbol{\tau}$ is the deviatoric stress tensor, and $\hat{\boldsymbol{\tau}}$ its Jaumann derivative, p' is the effective pressure, $J_{2\sigma}$ is the second invariant of the stress tensor, the subscripts tot, v, e, p mean, respectively, the total, viscous, elastic and plastic part of the strain tensor, η_n is a numerical viscosity, which is assigned by values large enough to vanish the viscous term of geomaterials in the solid state, η is the dynamic viscosity, μ' is the effective elastic shear modulus, and K_e' and K_v are the effective elastic and viscous bulk moduli, respectively.

After the time discretisation of $\dot{p}'$ and $\hat{\boldsymbol{\tau}}$ on the time step Δt_e, the global formulation is expressed as follows:

$$\begin{cases} \boldsymbol{\tau}^{t+\Delta t_e} = 2\eta_{eff}\left(\dot{\boldsymbol{e}}_{tot}^{\,t+\Delta t_e} - \dot{\boldsymbol{e}}_p^{\,t+\Delta t_e} \right) + \eta_{eff} \frac{\boldsymbol{\tau}^t}{\mu' \Delta t_e} + \eta_{eff} \frac{\left(\boldsymbol{W}^t \boldsymbol{\tau}^t - \boldsymbol{\tau}^t \boldsymbol{W}^t \right)}{\mu'} + \eta_{eff} \frac{s_y}{\eta} \frac{\boldsymbol{\tau}^t}{J_{2\sigma}^t} \\ p'^{t+\Delta t_e} = (K_v)_{eff} \left(\mathrm{tr}\left(\dot{\boldsymbol{\varepsilon}}_{tot}^{\,t+\Delta t_e} \right) - \mathrm{tr}\left(\dot{\boldsymbol{\varepsilon}}_p^{\,t+\Delta t_e} \right) + \frac{p'^t}{K_e' \Delta t_e} \right) \end{cases} \tag{30}$$

where $\eta_{eff} = \frac{1}{\frac{1}{\eta} + \frac{1}{\eta_n} + \frac{1}{\mu' \Delta t_e}}$ [2,10,28], different from the one in expressions (13), and $(K_v)_{eff}$ is the above-mentioned visco-elastic volumic

modulus (13). It should be noted that the plastic terms and the viscous term contributed by Bingham's yield stress s_y are considered explicitly [10]. Hence, a visco-elasto-plastic formulation is established by which problems involving plasticity can be solved by generalising the visco-elastic framework. Returning to our problem, the suction in unsaturated soils enhances the elastic moduli and gives soils greater initial strength. Both will be included, by introducing $p'^{t+\Delta t_e} = p^{t+\Delta t_e} + (\chi s)^{t+\Delta t_e}$ and effective elastic moduli depending on the suction, into the Eq. (30). The latters are expressed as in [27]:

$$\begin{cases} K'_e = \frac{p'_0}{k(1-n_0)} \\ \mu' = \frac{3(1-2\nu)p'_0}{2k(1+\nu)(1-n_0)} \end{cases} \tag{31}$$

where p'_0 is the initial effective isotropic consolidation pressure, ν is the Poisson's coefficient, n_0 is the initial porosity of the soil, and k a material parameter.

In the initial state, p'^t is assigned by the stress state due to the initial suction value so that the initial total mean pressure is nil, thus $p'^0 = \chi^0 s^0$. On one hand, the stress state of every particle is determined by the formulations at the end of every time step, on the other hand, it is determined with governing equation $\mathrm{div}\overline{\boldsymbol{\sigma}} = \mathrm{div}\boldsymbol{\sigma}' - \mathrm{grad}(\chi s) = \mathrm{div}\boldsymbol{\tau} + \mathrm{grad}p' - \mathrm{grad}(\chi s) = \boldsymbol{f}$:

$$2\eta_{eff}\left(\mathrm{div}\left(\dot{\boldsymbol{e}}_{tot}^{t+\Delta t_e}\right)\right) + (K_\nu)_{eff}\left(\mathrm{grad}\left(\mathrm{tr}\dot{\boldsymbol{\varepsilon}}_{tot}^{t+\Delta t_e}\right)\right) = \boldsymbol{f}' \tag{32}$$

The effective force $\boldsymbol{f}'$ is determined at the beginning of every time step, to compute the velocity field. On the basis of the relations above, $\boldsymbol{f}' = \boldsymbol{f}_1 + \boldsymbol{f}_2 + \boldsymbol{f}_3 + \boldsymbol{f}_4 + \boldsymbol{f}_5$, with:

- a term of the external force vector: $\boldsymbol{f}_1 = \boldsymbol{f}_{ext}^{t+\Delta t_e}$
- a term of the negative elastic force vector at time step t:

$$\boldsymbol{f}_2 = -\eta_{eff}\left(\mathrm{div}\left(\frac{\boldsymbol{\tau}^t}{\mu'\Delta t_e}\right)\right) - \eta_{eff}\left(\mathrm{div}\left(\frac{\boldsymbol{W}^t\boldsymbol{\tau}^t - \boldsymbol{\tau}^t\boldsymbol{W}^t}{\mu'}\right)\right) - (K\nu)_{eff}\left(\mathrm{grad}\left(\frac{p'^t}{K'_e\Delta t_e}\right)\right) \tag{33}$$

- a term of the positive plastic force vector at the previous time step t, after an explicit simplification:

$$\boldsymbol{f}_3 = 2\eta_{eff}\left(\mathrm{div}\left(\dot{\boldsymbol{e}}_p{}^t\right)\right) + (K_\nu)_{eff}\left(\mathrm{grad}\left(\mathrm{tr}\dot{\boldsymbol{\varepsilon}}_p{}^t\right)\right) \tag{34}$$

- a term of the force vector owing to Bingham yield stress s_y at the previous time step t:

$$\boldsymbol{f}_4 = -\frac{\eta_{eff}s_y}{\eta}\mathrm{div}\left(\frac{\boldsymbol{\tau}}{J_{2\sigma}}\right)^t \tag{35}$$

- a term of the force vector due to suction at the current time step $t + \Delta t_e$:

$$\boldsymbol{f}_5 = \mathrm{grad}(\chi s)^{t+\Delta t_e} \tag{36}$$

Ultimately, the visco-elasto-plastic formulation is resolved in an Euler-implicit/explicit scheme, implicit for the differential expression and for taking suction into account, explicit in consideration of the plasticity and Bingham's stress threshold.

4. Benchmarks

As an innovative hybrid finite element method, FEMLIP is considered to be a powerful numerical tool for simulating elasto-plastic materials with large transformations. The materials studied are initially discretised by Eulerian mesh and a series of material points, the latters carry different internal variables. The unknown quantity, such as the velocity field, is calculated in computational nodes of the fixed mesh. Since the material points are used as integration points, the velocity is interpolated from the computational nodes to the material points at the end of each time step. Consequently, the material points move according to the velocity field and the internal variables are refreshed locally. As the material properties are stored at the material points, and the numerical weights of integration points are refreshed by means of a particular algorithm at the end of each step [30], the accurate description of the material properties during the advection process is assured.

FEMLIP has been largely validated for various cases of viscous, visco-elastic and elasto-plastic materials, for instance: (1) linear visco-elasticity, such as the deflection of a visco-elastic beam [30]; (2) non-linear visco-elasticity depending on the accumulated strain, such as the geological evolution of a fold in a non-linear visco-elastic material [29], and (3) the behaviour of an elasto-plastic material, such as the isochoric compression of a homogeneous confined soil [32]. It has successfully simulated the whole process of a one-phase mudflow, including the elasto-plastic state before failure and the visco-elastic state after failure [28].

In this paper, three benchmarks are proposed to test the implementation of the new hydromechanical coupling in FEMLIP. It should first be noted that, it is necessary to distinguish material points in two types. Some do not involve or track hydraulic variables. For these particles, suction and all the other hydraulic variables are always nil, by switching off the shape function of water pressure. This means that the finite element formulation integrated by these particles is expressed as $\boldsymbol{A}\dot{\boldsymbol{U}} = \boldsymbol{F}$. The others involve hydromechanical coupling, in which the water pressure is refreshed and the suction–water content relationship is calculated in every computational time step. The corresponding formulation is thus Eq. (27).

4.1. Simple compression test

In a $2 \times 1m^2$ rectangle meshed by 8×4 elements, a weightless unsaturated soil is considered. A visco-elastic weight, whose dynamic viscosity η is infinitely large to vanish the viscous effect, with a gravity linearly increasing from 0 to 10 m/s^2, is applied on top to exert the vertical force. "Air" fills the remaining domain. The geometry is illustrated in Fig. 5(a).

Consequently, the soil sample has two fixed and free slip boundaries, one mobile boundary on the right, and is charged by a vertical force on the upper boundary. The model will be also used in Section 4.2 to exhibit the effect of imbibition.

Throughout the process of this test, the water flux boundary conditions maintain inactive. Elasto-plastic and hydraulic parameters are given in Tables 1 and 2.

Since the kinematic field is continuous in FEMLIP, a material point far enough from the visco-elastic weight on the top is chosen as a specimen, to avoid the influence of the visco-elastic weight on the strain. In Fig. 5(b), solid, dotted and dashed curves present the relation between the horizontal strain ε_{11} and the deviatoric stress q of this point, under different initial suctions $s_0 = 0$, $s_0 = 15$ kPa and $s_0 = 20$ kPa, respectively. There are several interesting points to note:

1. With increasing suction values, the elastic limit is extended.
2. With increasing suction values, the reached maximum of deviatoric stress q is increased.
3. The enhancement of the elastic modulus is closely observed, after the modification of the elastic moduli μ' and K'_e due to increasing suction values.

The three phenomena are explained as follows.

According to Bishop's effective stress expressed by Eq. (1), a higher initial suction gives a higher initial effective pressure p'_0.

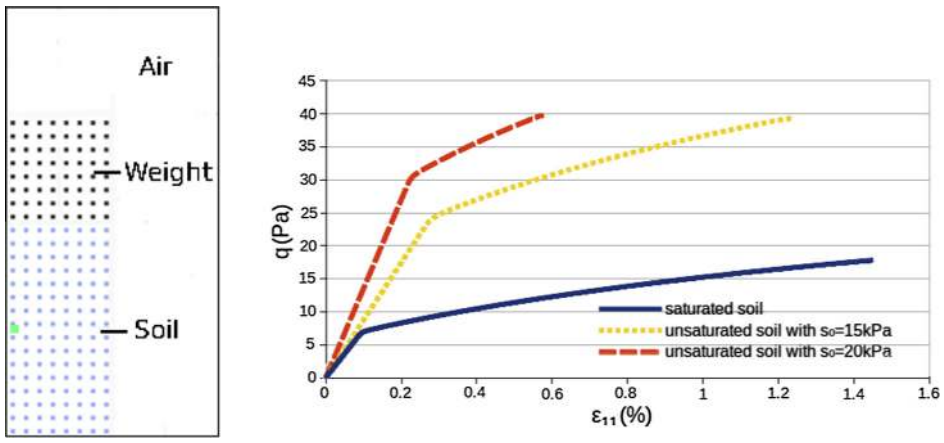

Fig. 5. (a) Geometry for the simple compression test and (b) predicted results of a simple compression test for a geomaterial specimen under different suction conditions (0, 15 and 20 kPa).

Table 1
Elasto-plastic parameters of the simple compression test.

Materials	E	ν	$\varphi_{e0}=\varphi_{c0}$	C_0	$\varphi_{ef}=\varphi_{cf}$	C_f	$\psi_e=\psi_c$	B_p	B_c	ρ
Unit	MPa	–	°	kPa	°	kPa	°	–	–	kg/m^3
EP soil	5	0.35	20	2	32	8	10	0.01	0.02	0
Weight	5	0.35	–	–	–	–	–	–	–	4000

Table 2
Hydraulic parameters of the simple compression test.

Parameters of Van Genuchten's WRCs						Hydromechanical coupled parameters			
a_d	n_d	a_w	n_w	Sr_{sat}	Sr_{res}	a_χ	n_χ	λ	n_0
1.602	1.38	1.602	1.38	1	0	0.6805	1.5847	0	0.39

The yield surface and the Van Eekelen plastic criterion have conical shapes. Consequently, a higher p'_0 along the hydrostatic line in the PLASOL model, as in Fig. 3, corresponds to a higher elastic limit and plastic limit. The PLASOL model using Bishop's effective stress describes the two typical features of unsaturated soils in a direct way. Eq. (30) also explains the increase of the elastic moduli with p'_0, which is observed in Fig. 5(b).

Furthermore, the increased suction leads to an inter-granular cementation, which is compatible with increased cohesion due to the suction, generally expressed on the basis of Bishop's effective stress:

$$\boldsymbol{\tau} = c' + \boldsymbol{\sigma}'\mathrm{tg}\varphi' = (c' + \chi s \mathrm{tg}\varphi') + \overline{\boldsymbol{\sigma}}\mathrm{tg}\varphi' \tag{37}$$

where c' and φ' are, respectively, effective cohesion and effective friction angle; $c = c' + \chi s \mathrm{tg}\varphi'$ is the apparent cohesion.

4.2. Imbibition test under pressure

The model in Fig. 5(a) is used here to present the influence of imbibition in the prefailure stage for unsaturated soils. The mesh is refined in 20×10 m^2, in order to ensure the accuracy of calculation. Firstly, a vertical force is exerted by increasing the gravity of the visco-elastic weight from 0 to 10 m/s^2 in 1000 δt ($\delta t = 0.00099$ s). Once the elapsed time is longer than 1 s, the vertical force remains constant and a homogeneous imbibition, by introducing a water flux of 6.24×10^{-5} m/s in each element, is then applied to the soil sample, until the test is finished. The initial suction value is 20 kPa, Bingham's yield stress s_y is infinitely large to ensure that the sample always stays in the solid state, and all the parameters are given in Tables 3 and 4. In Figs. 6 and 7, the dashed, dotted and solid curves present, respectively, results in a central soil particle, a soil particle within the fixed boundary and a soil particle in the free boundary. These three particles are located at the same level as the material point in Section 4.1.

Table 4
Viscous parameters of undrained triaxial test.

η (Pa s)	s_y (kPa)
50	0.1

Fig. 6(a) shows the relation between the effective pressure p' and $J_{2\sigma}$. With the increasing vertical force, p' and $J_{2\sigma}$ vary. p' reduces with a homogeneous imbibition for a given total pressure p, after $t > 1$ s. A slight reduction of suction and a contrary trend in the degree of saturation before $t < 1$ s are observed in Fig. 7, due to the contraction of intergranular voids. Then the suction decreases rapidly with the imbibition, and the degree of saturation presents the contrary tendency. In addition, suction and degree of saturation at different points coincide, because of the homogeneous imbibition and the independence of the degree of saturation on porosity ($\lambda = 0$). For this simulation, there is one phenomenon to point out: the particle near the fixed boundary shows a larger p' and $J_{2\sigma}$, and near the free boundary a smaller stress is observed.

Table 3
Elasto-plastic parameters of undrained triaxial test.

E (MPa)	ν	$\varphi_{e0}=\varphi_{c0}$ (°)	C_0 (kPa)	$\varphi_{ef}=\varphi_{cf}$ (°)	C_f (kPa)	$\psi_e=\psi_c$ (°)	B_p	B_c
2.5	0.2	1	1	28	10	5	0.01	0.02

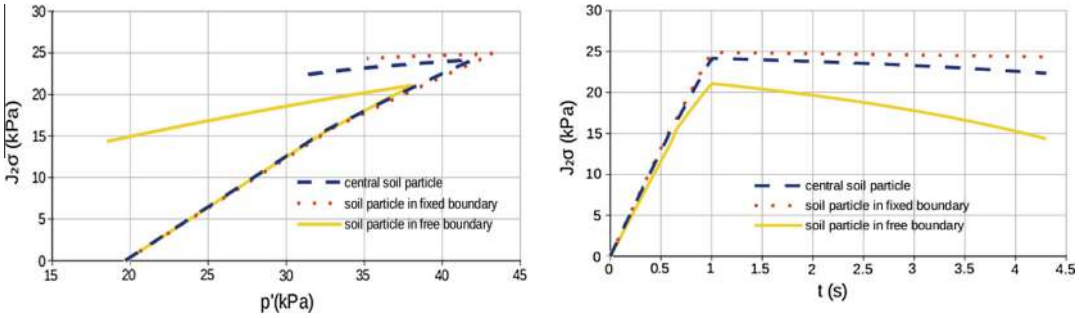

Fig. 6. (a) Effective stress path of three representative soil particles and (b) variation of $J_{2\sigma}$ over time for the same soil particles.

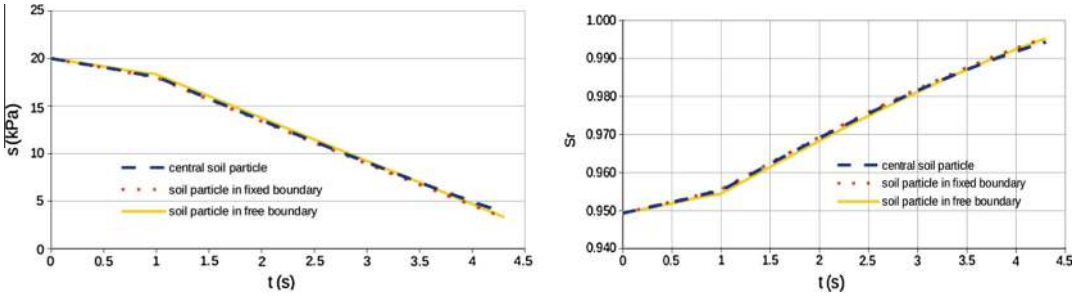

Fig. 7. (a) Suction and (b) degree of saturation over time.

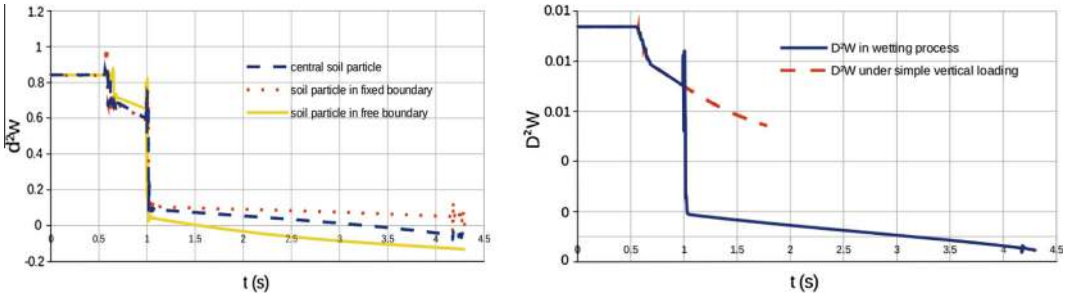

Fig. 8. (a) Evolution of d^2w over time in three representative soil particles and (b) evolution of global second-order work in different loading conditions.

Consequently, the stress field shows a continuous reduction from left to right, because the fixed boundary condition restricts the displacement in the horizontal direction, but on the right, the particles move freely, so that the development of plastic deformation is limited. This induces heterogeneous stress and strain fields with the development of the plastic strain. Fig. 8(a) gives a similar heterogeneity of d^2w for the above-mentioned reason. The sharp drop and the following decrease of d^2w due to the imbibition are observed in $t = 1$ s and afterwards. In Fig. 8(b), the evolution of global second-order work D^2W (the dashed curve) is shown. The vanishing due to the imbibition observed in $t = 3$ s, is almost the same as the vanishing of the local d^2w in the central particle. In addition, another simulation, in which the wetting load is not exerted after $t = 1$ s and the gravity increases at the same rate ($+0.01$ m/s^2 per time step), has been done: the solid curve shows that D^2W decreases without any sharp drop.

4.3. Undrained triaxial test with transition between solid–fluid states

In this simulation, an undrained triaxial test controlled by boundary wall velocities is modelled. Similar phenomena due to increasing suction values are surveyed. Moreover, the solid–fluid transition is activated, and the target behaviours are illustrated.

This model comprises a homogeneous geomaterial sample measuring 1×1 m^2 with 4×4 elements. The kinematic boundary conditions controlled in two stages are illustrated in Fig. 9. Firstly, horizontal velocity (x-axis) and vertical velocity (y-axis) are applied to the sample isotropically ($V_x = V_y = 0.6$ m/s), so that the sample undergoes the same strains $\varepsilon_{xx} = \varepsilon_{yy} = 0.001$ in both directions. Until net confining pressure $p = 3$ kPa is attained, the second stage starts, and the horizontal velocity reverses in order to maintain an isochoric condition, that is to say: $\varepsilon_{xx} + \varepsilon_{yy} = 0$. As in the previous test, throughout the process, the water flux boundary conditions remain inactive, meaning that the suction tends to decrease in the first stage because of the isotropic compression, and is maintained constant in the second one.

The visco-elasto-plastic and hydraulic parameters are enumerated in Tables 3–5. Fig. 10 shows the relation between the effective pressure and the second invariant of the stress tensor, with a solid–fluid transition. In the figure, the curves represent saturated soil and unsaturated soil under a 10 kPa suction. Initially, the effective confining pressure and $J_{2\sigma}$ increase in the isotropic consolidation stage, because of a plane deformation hypothesis (while $q = \sigma_{xx} - \sigma_{yy}$ remains zero). Then $J_{2\sigma}$ increases rapidly while p'

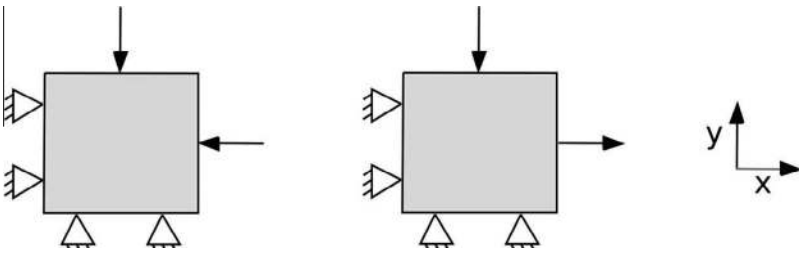

Fig. 9. (a) Isotropic consolidation stage and (b) deviatoric loading stage under isochoric condition.

Table 5
Hydraulic parameters of undrained triaxial test.

Parameters of Van Genuchten's WRCs						Hydromechanical coupled parameters			
a_d	n_d	a_w	n_w	Sr_{sat}	Sr_{res}	a_χ	n_χ	λ	n_0
1	1.35	10	1.35	1	0.1	2	2.15	0.5	0.4

remains constant until the elastic limit is attained, as is expected from an isotropic elastic behaviour. As a contractant material according to its physical parameters, once entering the elasto-plastic domain, p' starts to decrease. When $J_{2\sigma}$ reaches the peak value, we have $dJ_{2\sigma} = 0$ and $d\varepsilon_v = 0$ (isochoric loading). According to Hill's second-order work d^2w and Bingham's yield stress s_y, respectively:

$$\begin{cases} d^2w = dJ_{2\sigma}d\varepsilon_d + dp'd\varepsilon_v = 0 \\ J_{2\sigma} > s_y \end{cases} \tag{38}$$

the diffuse failure thus occurs in the bifurcation domain, as illustrated by the solid curves. In Fig. 10, obviously, the unsaturated soil exhibits a higher peak of deviatoric stress and a larger elastic domain. The diffuse failure comes later due to a larger apparent cohesion.

Fig. 11 presents the variation of $J_{2\sigma}$ over physical time. As in the saturated soil, the $J_{2\sigma}$ of the unsaturated soil falls below s_y, while diffuse failure is attained, which corresponds to the fact that fluids do not support a deviatoric stress beyond the yield stress s_y. Furthermore, the properties depending on the suction, such as the larger elastic domain, the greater strength and failure occurring later are observed in Fig. 11.

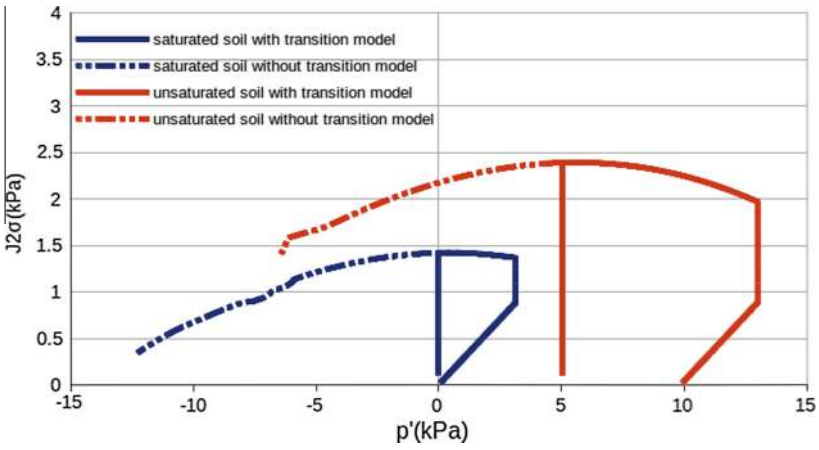

Fig. 10. Effective stress paths of saturated and unsaturated soils (s = 10 kPa) with (solid lines) or without (dashed lines) transition.

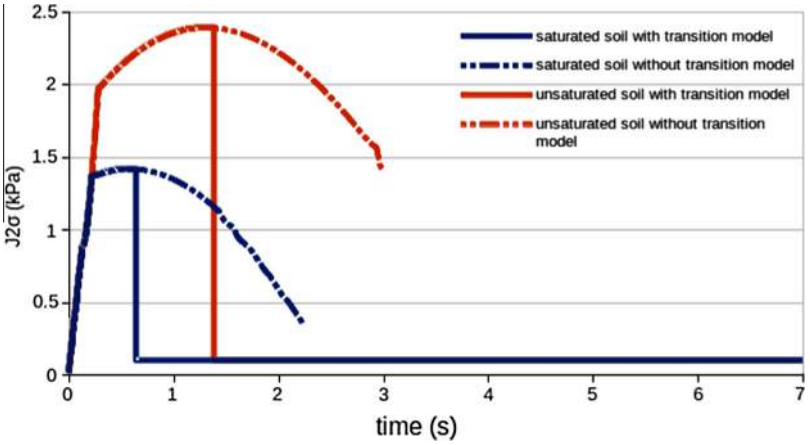

Fig. 11. Variation of $J_{2\sigma}$ over time in saturated and unsaturated cases.

5. Conclusions

In this paper, a new finite element formulation for solving fully coupled hydromechanical problems is developed in the FEMLIP visco-elasto-plastic framework, by introducing assumptions as follows: (1) the liquid and solid phases are incompressible; (2) the heat transfer is neglected and the temperature field is assumed to be constant; (3) the generalised Darcy's law is used to describe the liquid flowing in the connected voids of the medium; (4) the air pressure and the water vapour pressure are considered nil, under atmospheric air pressure. On this basis, the stress–strain relation for unsaturated soils is derived by introducing Bishop's effective stress into the PLASOL elasto-plastic model. The modified Van Genuchten's WRCs linking the degree of saturation to suction and porosity is implemented, from which the suction–water content relation is derived. For taking into account the non-symmetry of the numerical operator, a new solver based on the biconjugate gradient stabilised method has also been implemented.

The capacity of the model to deal with coupled hydromechanical problems has been validated by three benchmarks, focusing on three aspects: (1) features of unsaturated soil, for instance, enhancements of the deviatoric stress peak and elastic modulus in Section 4.1, (2) the diffuse failure due to the imbibition and the dependence on boundary conditions to integrate the global second-order work, in Section 4.2, and (3) the sharp drop in deviatoric stress and the fluid-like behaviour observed in postfailure stage in Section 4.3.

In conclusion, the model appears to be reliable to describe unsaturated soil behaviours both in prefailure and postfailure stages. Unfortunately, to the author knowledge, there is no experimental results at the Laboratory scale on a sample loaded in plane strain under hydromechanical conditions. Thus the validation is only qualitative. By improving essentially the fluid-like model, and by taking into account inertial forces for rapid flow, more realistic cases, for example, unsaturated slopes and rainfall-induced landslides of the flow type (mudflows, debris flows) can be simulated.

References

[1] Dufour F. Développements de la méthode des éléments finis avec des points d'intégration Lagrangiens: Applications à la géomécanique. Ph.D. Thesis. Ecole centrale de Nantes; 2002.
[2] Prime N. Modélisation de la transition solide-fluide dans les géomatériaux. Application aux glissements de terrain. Ph.D. Thesis. Université de Grenoble; 2012.
[3] Van Genuchten MT. A closed-form equation for predicting the hydraulic conductivity of unsaturated soils. Soil Sci Soc Am J 1980;44:892–8.
[4] Alonso EE, Gens A, Josa A. A constitutive model for partially saturated soils. Géotechnique 1990;40(3):405–30.
[5] Cui YJ, Delage P. Yielding and plastic bahviour of an unsaturated compacted silt. Géotechnique 1996;46(2):291–311.
[6] Bolzon G, Schrefler BA, Zienkiewicz OC. Elastoplastic soil constitutive laws generalised to partially saturated states. Géotechnique 1996;46(2):279–89.
[7] Pastor M, Zienkiewicz O, Chan A. Generalized plasticity and the modelling of soil behaviour. Int J Numer Anal Methods Geomech 1990;14:151–90.
[8] Gallipoli D, Gens A, Sharma R, Vaunat J. An elasto-plastic model for unsaturated soil incorporating the effects of suction and degree of saturation on mechanical behaviour. Géotechnique 2003;53(1):123–35.
[9] Barnichon JD. Finite element modelling in structural and petroleum geology. Ph.D. Thesis. University of Liege; 1998.
[10] Prime N, Dufour F, Darve F. Unified model for geomaterial solid/fluid states and the transition in between. J Eng Mech 2014;140(6):682–94.
[11] Wheeler SJ, Sharma RJ, Buisson MSR. Coupling of hydraulic hysteresis and stress–strain behaviour in unsaturated soil. Geotechnique 2003;53(1):41–54.
[12] Tarantino A, Sacchet A, Dal Maschio R, Francescon F. A hydromechanical approach to model shrinkage of air-dried green body. J Am Ceram Soc 2010;93:662–70.
[13] Hill R. A general theory of uniqueness and stability in elastic–plastic solids. J Mech Phys Solids 1958;6:236–49.
[14] Van Eekelen HAM. Isotropic yield surface in three dimensions for use in soil mechanics. Int J Numer Anal Methods Geomech 1980;4(1):89–101.
[15] Taylor D. Fundamentals of soil mechanics. London: Wiley; 1948.
[16] Darve F, Servant G, Laouafa F, Khoa HDV. Failure in geomaterials: continuous and discrete analyses. Comput Methods Appl Mech Eng 2004;193(27–29):3057–85.
[17] Khoa HDV, Georgopoulos IO, Darve F, Laouafa F. Diffuse failure in geomaterials. Comput Geotech 2006;33:1–14.
[18] Laouafa F, Prunier F, Daouadji A, Al Gali H, Darve F. Stability in geomaterials, experimental and numerical analyses. Int J Numer Anal Methods Geomech 2011;35:112–39.
[19] Prunier F, Laouafa F, Lignon S, Darve F. Bifurcation modelling in geomaterials: from the second-order work criterion to spectral analyses. Int J Numer Anal Methods Geomech 2009;33:1169–202.
[20] Nicot F, Daouadji A, Laouafa F, Darve F. Second-order work, kinetic energy and diffuse failure in granular materials. Granul Matter 2010;13:19–28.
[21] Balmforth NJ, Craster RV. A consistent thin layer theory for Bingham plastics. J Non-Newton Fluid Mech 1999;84(1):65–81.
[22] Nuth M, Laloui L. Effective stress concept in unsaturated soils: clarification and validation of a unified framework. Int J Numer Anal Methods Geomech 2008;32:770–801.
[23] Laloui L, Nuth M. On the use of the generalised effective stress in the constitutive modelling of unsaturated soils. Comput Geotech 2009;36:20–3.
[24] Bishop AW. Principle of effective stress. Teknisk Ukeblad 1959;106 (39):859–63.
[25] Khalili N, Khabbaz M. A unique relationship for χ for determination of the shear strength of unsaturated soils. Géotechnique 1998;48(5):681–7.
[26] Alonso EE, Pereira JM, Vaunat J, Olivella S. A microstructurally based effective stress for unsaturated soils. Géotechnique 2010;12:913–25.
[27] Arairo W, Prunier F, Djéran-Maigre I, Darve F. A new insight into modelling the behaviour of unsaturated soils. Int J Numer Anal Methods Geomech 2013;37:2629–54.
[28] Prime N, Dufour F, Darve F. Solid–fluid transition modelling in geomaterials and application to a mudflow interacting with an obstacle. Int J Numer Anal Methods Geomech 2014;38(13):1341–61.
[29] Muhlhaus H-B, Moresi L, Hobbs B, Dufour F. Large amplitude folding in finely layered viscoelastic rock structures. Pure Appl Geophys 2002;159 (10):2311–33.
[30] Moresi L, Dufour F, Muhlhaus H-B. A Lagrangian integration point finite element method for large deformation modelling of viscoelastic geomaterials. J Comput Phys 2003;184:476–97.
[31] Moresi L, Dufour F, Muhlhaus H-B. Mantle convection modeling with viscoelastic/brittle lithosphere: numerical methodology and plate tectonic modeling. Pure Appl Geophys 2002;159(10):2335–56.
[32] Cuomo S, Prime N, Iannone A, Dufour F, Cascini L, Darve F. Large deformation FEMLIP drained analysis of a vertical cut. Acta Geotech 2013;8(2):125–36.
[33] Sulsky D, Zhou SJ, Schreyer HL. Application of a particle-in-cell method to solid mechanics. Comput Phys Commun 1995;87(1–2):236–52.
[34] Muraleetharan KK, Liu C, Wei C, Chen L. An elastoplastic framework for coupling hydraulic and mechanical behaviour of unsaturated soils. Int J Plast 2009;25(3):473–90.
[35] Sheng D, Sloan SW, Gens A. A constitutive model for unsaturated soils: thermomechanical and computational aspects. Comput Mech 2004;33 (6):453–65.
[36] Duvaut G, Lions JL. Transfert de chaleur dans un fluide de Bingham dont la viscosité dépend de la température. J Func Anal 1972;11(1):93–110.
[37] Khoa HDV. Modélisation des glissements de terrain comme un problème de bifurcation. Ph.D. Thesis. Institut National Polytechnique de Grenoble; 2005.
[38] Scholtès L, Hicher P-Y, Nicot F, Chareyre B, Darve F. On the capillary stress tensor in wet granular materials. Int J Numer Anal Methods Geomech 2009;33 (10):1289–313.
[39] Scholtès L, Chareyre B, Nicot F, Darve F. Micromechanics of granular materials with capillary effects. Int J Eng Sci 2009;47(1):64–75.
[40] Sheng D, Gens A, Fredlund DG, Sloan SW. Unsaturated soils: from constitutive modeling to numerical algorithms. Comput Geotech 2008;35(6):810–24.
[41] Van der Vorst HA. Bi-CGSTAB: a fast and smoothly converging variant of Bi-CG for the solution of nonsymmetric linear systems. SIAM J Sci Comput 1992;13 (2):631–44.
[42] Cascinia L, Cuomoa S, Pastor M, Sorbinoa G, Piciulloa L. SPH run-out modelling of channelised landslides of the flow type. Geomorphology 2014;214:502–13.
[43] Abe K, Soga K, Bandara S. Material point method for coupled hydromechanical problems. J Geotech Geoenviron Eng 2014;140(3):682–700.
[44] Mualem Y. A conceptual model of hysteresis. Water Resour Res 1974;10:514–20.